FLOW STRUCTURES AND PRESSURE FLUCTUATIONS IN A TIP LEAKAGE FLOW

Roberto Camussi[1] , Marc C. Jacob[2] , Julien Grilliat[1,2] and Giovanni Caputi-Gennaro[1]

[1] *Mechanical and Industrial Engineering Dept. (DIMI), University 'Roma 3', Rome, I-00146, Italy*
E-mail: *camussi@uniroma3.it, jgrilliat@uniroma3.it*
[2] *Centre Acoustique du LMFA ,UMR CNRS 5509 – Ecole Centrale de Lyon – Université Claude-Bernard Lyon I, F- 69134 Ecully Cedex, France*
E-mail: *marc.jacob@ec-lyon.fr*

Keywords: wall pressure, tip leakage flow, wavelet, acoustics.

SUMMARY. Advanced post-processing techniques based on the wavelet transform are applied to pressure signals measured at the surface of an instrumented airfoil installed within the anechoic wind tunnel available at the Laboratory of Fluid Mechanics and Acoustics of the Ecole Centrale de Lyon. Two flow configurations, with and without a variable gap at the airfoil tip, are investigated. The scope of the post-processing procedure is to extract the most energetic non-periodic contributions, localized in time and in space, and to detect the fluid dynamic structures which may act as noise sources. The events tracking method is based on the computation of time-frequency energy maps from which it is possible to select events, determine their time of appearance, and perform conditional averages. The conditioning procedure has shown that the amplitude of the oscillations of the averaged pressure signature becomes larger for increasing width of the gap, probably as an effect of a roll-up phenomenon occurring at the tip edge of the airfoil. In addition, the pressure-velocity cross analysis, including data obtained from PIV measurements, yielded the location of the major fluid dynamic structure statistically related to the largest pressure fluctuations at the wall.

NOMENCLATURE

a	=	geometrical angle of attack
c	=	chord length
C_Ψ	=	dimensionless coefficient in the wavelet expansion
i	=	time index
f	=	frequency
p	=	pressure
r	=	resolution time scale
t	=	translation time
U_0	=	inflow speed
w	=	wavelet coefficients
x	=	distance from the leading edge (LE) in chord-wise direction
z	=	distance from the tip edge in span-wise direction

[1] Associate Professor, DIMI, University 'Roma 3', Via della Vasca Navale 79, Rome, I-00146, Italy.
[2] Assistent Professor, LMFA, Ecole Centrale de Lyon, 36 avenue Guy de Collongues, 69134 Ecully Cedex, France.

Ψ = mother wavelet function

1 INTRODUCTION

During the last decades, wavelet analysis has been extensively used to analyze random data obtained from both numerical simulations and experimental investigations conducted in turbulent flows. Comprehensive reviews about the wavelet theory and applications can be found in many reference papers or books (e.g. see among many [1] and [2]). Conditional sampling techniques based on the wavelet transform have been applied to turbulence data [3] and to pressure velocity measurements [4] in order to extract the most energetic contributions of the original signals. In the present work, a wavelet based post-processing methodology is applied to pressure and velocity data measured on an instrumented airfoil installed within the anechoic wind tunnel available at the Laboratory of Fluid Mechanics and Acoustics of the Ecole Centrale de Lyon. The purpose of the study is to investigate the physical nature of the cause of the largest pressure fluctuations on the airfoil surface for both a self noise configuration and a fan-tip with clearance configuration. To this aim, a convenient wavelet-based post-processing technique is applied to experimental data permitting us to extract the most energetic non-periodic contributions to the pressure fluctuations, localized in time and in space and hidden in the original chaotic signals.

A conditional average procedure based upon the wavelet analysis has been applied to both the wall-pressure and velocity data delivered by the experimental campaign, in order to recover the most probable shape of the most energetic pressure events detected over the airfoil surface and to obtain a statistical correlation between the flow dynamics (described by either single probe hot-wire anemometer and PIV measurements) and the largest wall pressure fluctuations (extracted from the wavelet treatment of single point pressure signals). A detailed description of the experimental apparatus, the measurements technique, the acquisition parameters and the flow conditions are given in part one of this paper (see [5]). Here, we limit ourselves to describe the techniques adopted to analyze the experimental data and to present results which can be useful to better clarify physical mechanisms connected with the generation of the largest pressure fluctuations.

2 EXPERIMENTAL SET-UP

The experimental campaign was carried out in the anechoic tunnel of the Ecole Centrale de Lyon at a Mach number M ~ 0.2. Details on the experimental set up are given in [5] but, for the sake of clarity, the main features are briefly summarized in the following.

The airfoil was placed into an open-jet flow, which was limited in the span-wise direction by two flat plates. The gap between the lower plate and the airfoil tip was adjustable. A 5% camber thick (10%) airfoil was used in the experiment, that is a NACA 5510, with a 15° geometrical angle of attack as reference value. The chord was 200 mm and the span increased from 190 to 200 as the gap decreased from 10 to 0 mm.

The influence of various governing parameters was investigated in [5] by varying their values: the flow speed was increased from 20 to 90 m/s, the gap between the tip and the plate was varied from 0 to 10 mm and the angle of attack was varied between 0 and 18°. However here we concentrate mainly on two *reference configurations.* The former is a self-noise configuration (gap = 0) with the inflow speed U_0 and the angle of attack α set to 70 m/s and 15° respectively. In the following, it is referred to as the *no gap reference configuration.* The latter is characterized by a 10 mm gap width, again with U_0 = 70 m/s and α = 15°. In the following, it is denoted the *reference gap configuration.*

Unsteady pressure measurements on the airfoil, both in the mid-span region and in the gap region were combined with far field and single probe hot-wire anemometer (HWA) measurements.

A special care was given to placing the pressure probes on the tip of the airfoil, on the two tip edges and on the plate facing the tip. Moreover, two sets of pressure probes were installed in the mid-span region both chord-wise and span-wise near the trailing edge.

Simultaneous PIV and single point pressure measurements were carried out both around the airfoil and in the gap region. Of particular interest here are the PIV-pressure data measured on the reference gap configuration. In this case, the measurement plane was located in the mid-gap plane (5 mm away from the tip edge of the airfoil) and the laser source was placed on the pressure side. Two near field pressure probes were placed on the airfoil tip along the mean line of the profile, at 6 and 155 mm far from the leading edge. A third pressure probe was placed in the far field, about 1 m away from the airfoil centre, on the suction side in the mid-span plane.

The measurements were divided into 10 acquisition series. During each acquisition, 60 PIV snapshots were taken at a frequency of 1 Hz (which means 60 s per acquisition), while the pressure signals were sampled at 20 kHz. This yields a total of 600 PIV snapshots and 10 pressure series resulting from the experimental measurements.

3 WAVELET ANALYSIS AND THE AUTO-CONDITIONING METHOD

The post-processing procedure adopted therein is based on the wavelet transform of the wall pressure signals. The scope of the procedure is to extract the most energetic non-periodic contributions, localized in time and in space. The choice of the wavelet technique is motivated by the fact that the wavelet decomposition, in spite of the Fourier transform, permits to represent a generic signal simultaneously in terms of a translation time (t) and a resolution time scale (r), whose inverse corresponds to the frequency (f). The wavelet decomposition is accomplished by projecting the acquired signal over basis of compact support functions $\Psi(t)$, i.e. localized both in the time domain and in the transformed space. We note that in the Fourier decomposition the projection is performed over trigonometric functions, so that the physical information is spread over a theoretically infinitely extended time domain. Localized events are therefore missed by the Fourier decomposition while they are correctly retrieved by the wavelet transform through the representation of the signal over a two dimensional map in the time-frequency domain.

Formally, the wavelet transform of the signal $p(t)$ at the resolution time scale r is given by the following expression.

$$w(r,t) = C_{\Psi}^{-1/2} r^{-1/2} \int_{\infty}^{\infty} \Psi^{*}\left(\frac{t-\tau}{r}\right) p(\tau) d\tau \tag{1}$$

where $C_{\Psi}^{-1/2}$ denotes a coefficient which accounts for the mean value of $\Psi(t)$, and the integral represents a convolution between $p(t)$ and the dilated and translated complex conjugate counterpart of $\Psi(t)$.

The events tracking method is based on the computation of the so called Local Intermittency Measure [2] defined as:

$$LIM(r,t) = \frac{w(r,t)^2}{\left\langle w(r,t)^2 \right\rangle_t} \tag{2}$$

where the symbol $\left\langle \bullet \right\rangle_t$ denotes a time average. Figure 1 shows an example of LIM distribution computed for a portion of pressure signal recorded at the wall. It is worth noting that the numerator of eq. (2), i.e. square of the wavelet coefficients, represents the localized counterpart of the standard Fourier spectrum that can be recovered by simple time integration. An example of the

Fourier spectrum recovered from the square of the wavelet coefficients plotted against the standard Power spectrum is reported in Figure 2a while Figure 2b reports similar results obtained with different wavelet kernels, demonstrating that the choice of the wavelet type does not influence the achieved results. It has been also checked that the results are independent from the use of orthonormal discrete or continuous complex wavelets. Examples elucidating these comparisons are not presented here for the sake of brevity. In the following analyses, except for the case of PIV/pressure data, an orthogonal discrete wavelet expansion is performed on the pressure signals by using a Fast-Wavelet-Transform algorithm with the Battle-Lemarie Mother wavelet $\Psi(t)$.

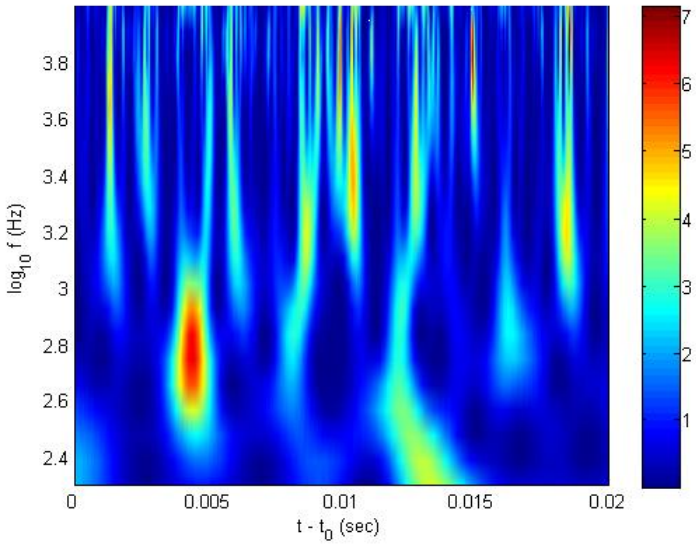

Figure 1. Example of LIM distribution computed for a portion of pressure signal recorded on the airfoil surface.

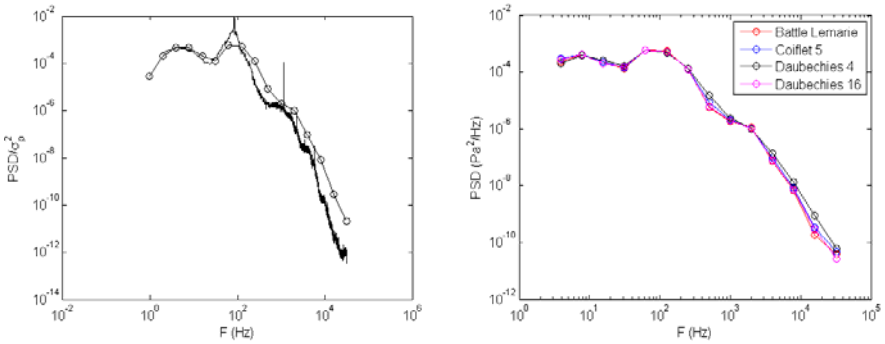

(a) **(b)**

Figure 2. Power spectrum obtained from the wavelet transform compared with a standard Fourier spectrum (a) and with results obtained adopting different types of mother wavelets (b).

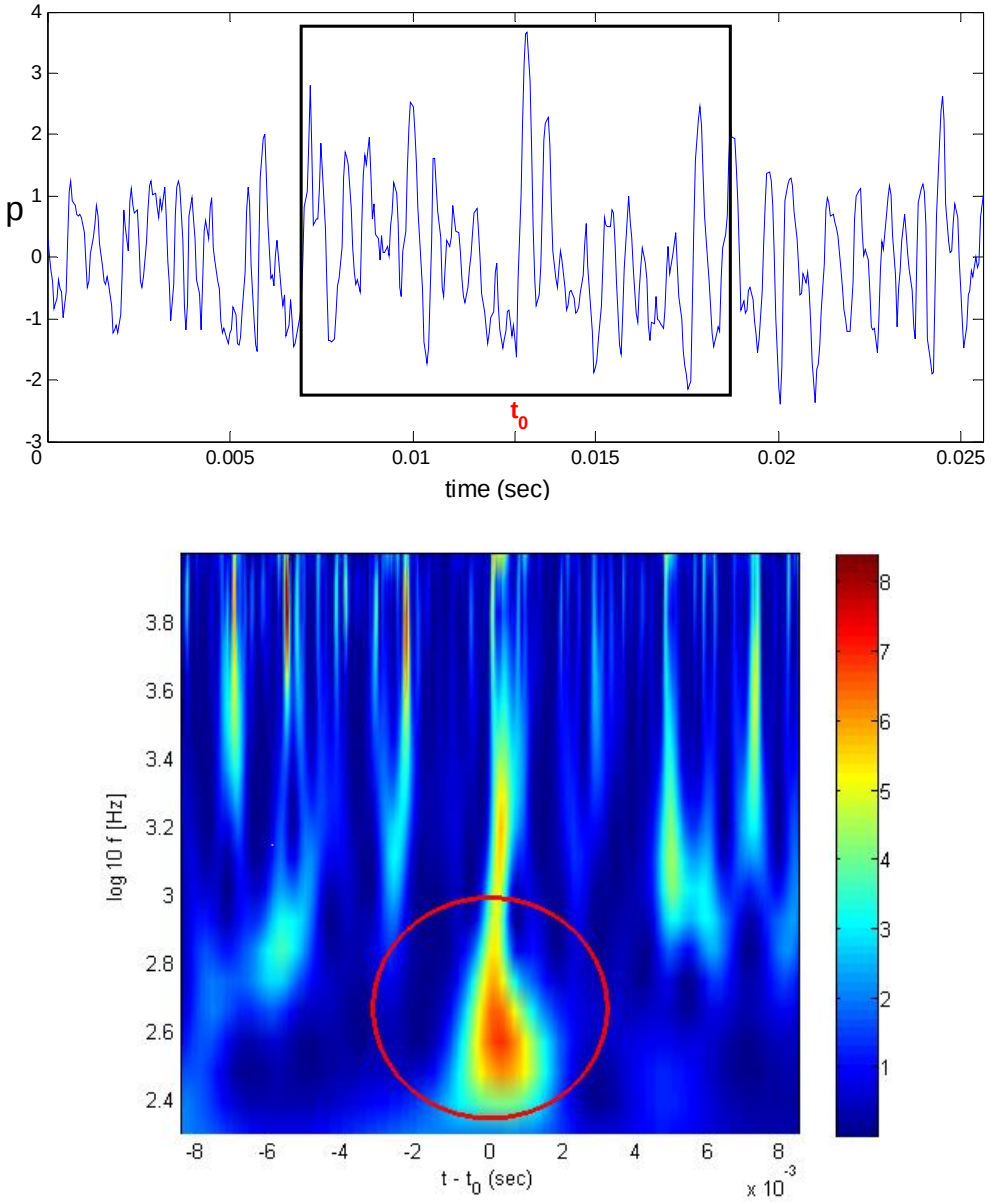

Figure 3. Selection procedure: the large value of LIM (red circle in the lower panel) indicates that an event occurs at the probe location in t = t0. Once the event is detected the portion of pressure signal centered in t0 is extracted to perform the conditional .average.

Peaks of LIM represent large contribution of pressure variations to the overall SPL. Therefore the LIM amplitude at a selected scale *r*, can be thresholded in order to select events responsible for the largest pressure fluctuations and to determine how their appearance is distributed in time (see Figure 3). Once the pressure events have been selected and well localized in the time domain, one may perform a conditional average of the original pressure signal. This auto-conditioning

procedure leads to an ensemble averaged time signature of the fluctuating pressure, which represents the most probable shape of the most energetic structures which are hidden in the original chaotic signal. The wavelet transform is indeed needed to recover the phase of the events responsible for the largest pressure fluctuations at the wall. The phase is a random non-periodic and strongly non-Gaussian variable and the averaged pressure signature, whenever it is non-zero, helps to clarify the fluid dynamic origin of the selected events. The original method was introduced in [3] and successively applied to pressure signals and validated in [4] while applications to wall pressure data were presented in [6].

4 WAVELET ANALYSIS AND THE AUTO-CONDITIONING METHOD

As clarified in section 2, velocity measurements using a single probe HWA have been conducted simultaneously to the wall pressure measurements in several configurations. Simultaneous PIV/pressure measurements have also been performed, in particular on the reference gap configuration. These experimental investigations provided useful data to perform a statistical analysis, which gives further clarifications on the physical nature of the fluid dynamic structures in the noise generation phenomenon. The conditioning method explained above has been applied to both the HWA/wall-pressure data and to the PIV/wall-pressure data, in order to extract aerodynamic events correlated to large localized pressure peaks at the wall of the airfoil.

In particular, once the pressure events have been selected and well localized in the time domain, the conditional average can be performed either on the single point velocity time series (HWA signals) or on the set of PIV snapshots available, provided that the velocity measurements are acquired simultaneously with the pressure signal analyzed. As a result, the outcome of the cross-conditional procedure analysis should be an averaged signature of velocity, representing the most probable fluid dynamic structure correlated to the pressure fluctuations at the wall of the airfoil.

5 RESULTS

5.1 *Auto-processing*

The auto-conditioning method provides the wall-pressure averaged signatures in several positions over the airfoil surface. In the no gap reference configuration, significant results are obtained only with the probes placed in the mid-span region. As clarified below, in this region the effect of the chord-wise position seems to be relevant.

An overall summary of results obtained considering probes located at mid-span ($z = 0$) for the no gap configuration is given in Figure 4. It is shown that the shape of the averaged signatures significantly changes with the x/c parameter. The behavior obtained close to the leading edge seems to indicate that acoustic effects are dominant with respect to hydrodynamic perturbations. This is an expected result since in the LE region the boundary layer is very thin and not yet developed so that acoustic perturbations, generated by the impact of the incoming unsteady flow against the airfoil surface, are the main sources of noise.

When we move towards the trailing edge (TE), a different behavior is observed, as shown in the x/c=0.25 case of Figure 4. Here a pressure drop is observed thus suggesting that, in a statistical sense, the pressure fluctuations are generated mostly by vortical structures passing close to the pressure probe position.

In the region close to the TE no significant results are obtained as an effect of the back-ground disturbance and the signal-to-noise ratio of the averaged pressure signatures is too low for any physical interpretations to be addressed.

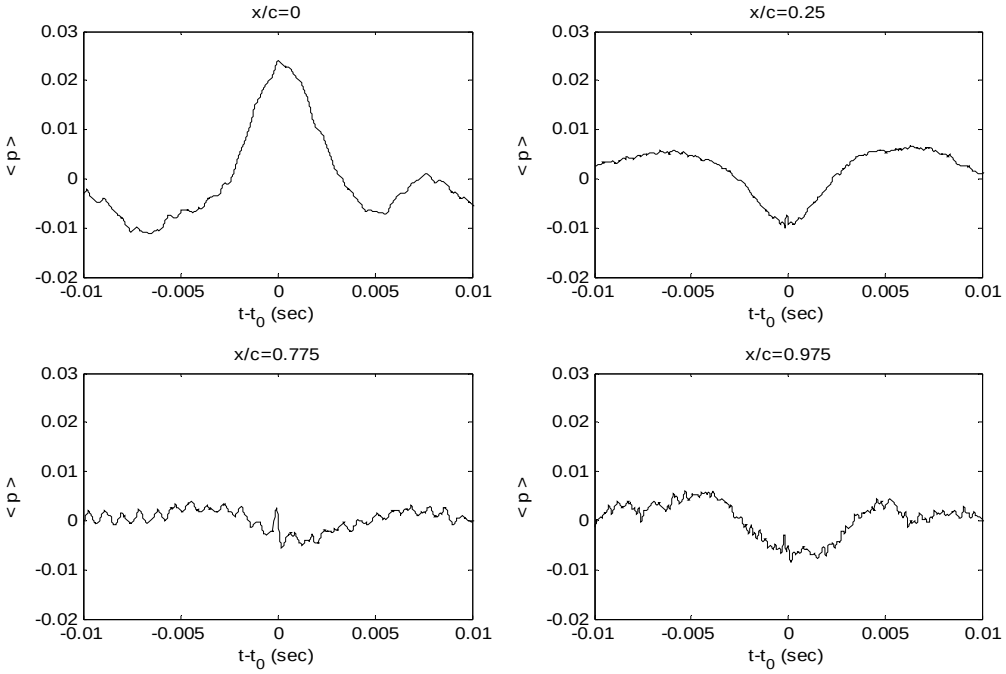

Figure 4. Averaged pressure time signatures obtained for several chord-wise positions at mid span for the no gap reference configuration.

No significant results are obtained also in the pressure side confirming that being the boundary layer very thin, the hydrodynamic perturbations induced by vortical structures are very weak and, from a statistical viewpoint, are uncoherent. An example of results obtained on the pressure side for the no gap reference configuration is given in Figure 5.

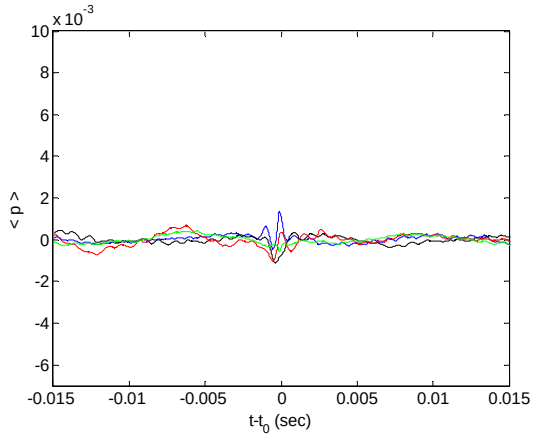

Figure 5. Examples of Averaged pressure time signatures obtained from several transducers in the pressure side of the airfoil for the no gap reference configuration.

The presence of a gap leads to pressure oscillations in the averaged signatures, as evidenced in Figures 6-7 for the reference gap configuration. In Figures 6 and 7(a) one may note that the oscillations are more pronounced close to the TE and at the edge of the airfoil in correspondence of the gap. Figures 7(b) shows that the amplitude of the oscillating averaged pressure signature becomes larger for increasing width of the gap, with both the angle of attack and the inflow speed kept fixed at their reference values.

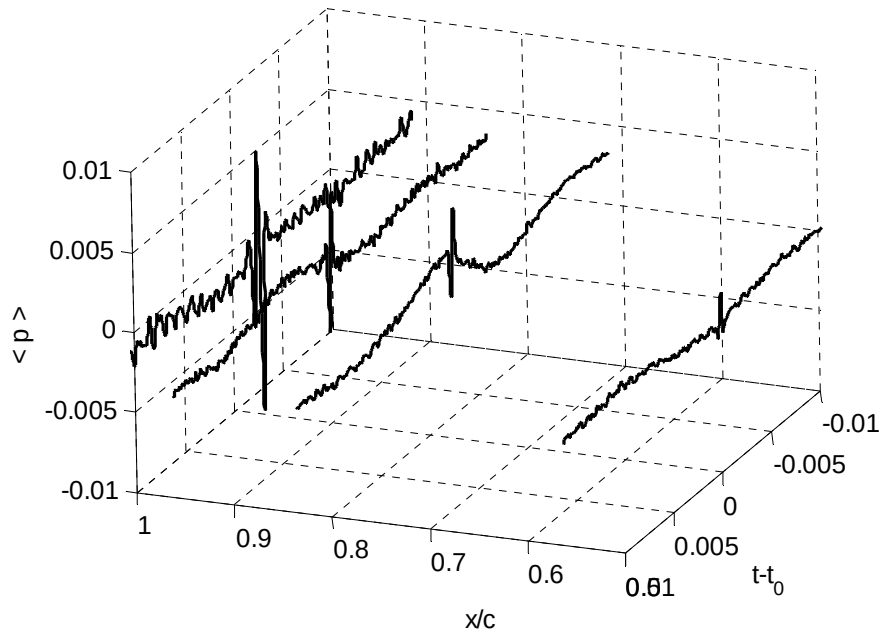

Figure 6. Averaged pressure time signatures obtained for several chord-wise positions in the tip region for the reference gap configuration.

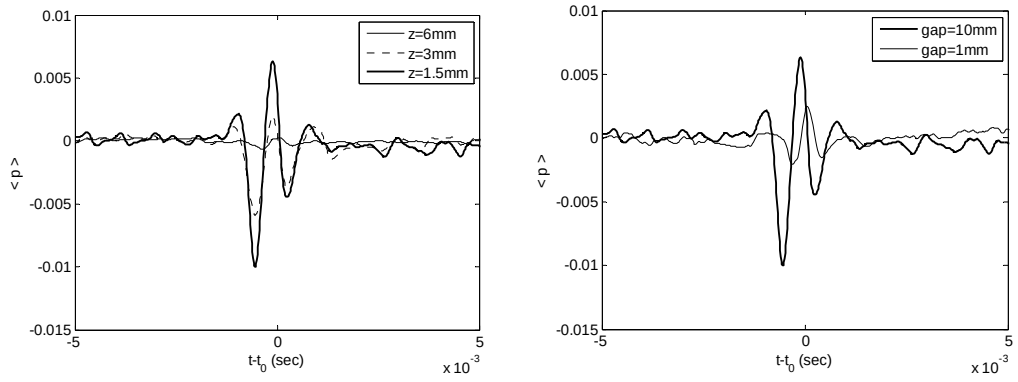

Figure 7. Averaged pressure time signatures obtained in the trailing edge region for the reference gap configuration: (a) effect of the distance from the gap (z), (b) effect of the gap width, with U_0 and α kept fixed at their reference values.

The observed behavior is due, probably, to vortex shedding from the side edge of the airfoil but, being such an effect not evident in the pressure power spectra, it has to be attributed to intermittent unsteady events which are not revealed when the signal is projected onto the Fourier basis. The physical nature of the observed phenomenon could be found into the mechanism of roll up of the vortical structures shed from the lower side of the airfoil and further insights would be inferred from the cross-analysis of the next sections.

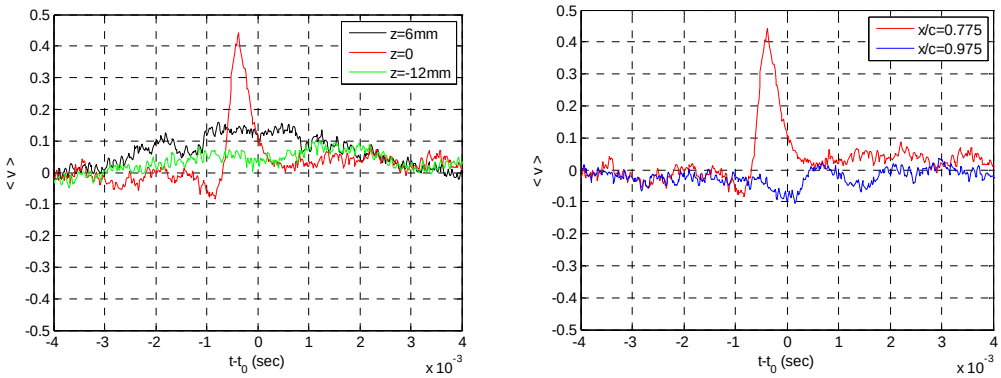

(a) **(b)**

Figure 8. Pressure-velocity correlation for the no gap reference configuration: (a) in the trailing edge region, (b) in the mid-span region.

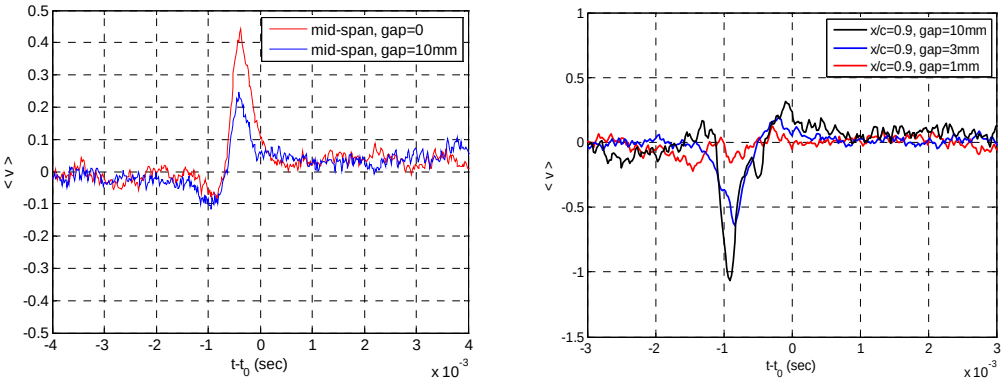

(a) **(b)**

Figure 9. Effect of the gap on the pressure-velocity correlation at the trailing edge (x/c = 0.975): (a) mid-span region: effect of the gap, (b) tip edge region.

5.2 *Pointwise velocity/Pressure conditional statistics*

As discussed in section 2, simultaneous velocity/pressure measurements have been performed by placing a single hot wire probe close to the airfoil trailing edge at a mid-span location. The results obtained from the cross-conditioning procedure for both the reference configurations are presented. In Figure 8 the averaged velocity signatures for the no gap reference configuration are depicted: the HWA signal has been conditioned by extracting the pressure events in several

locations along the trailing edge and in the mid-span region. A relevant pressure velocity correlation can be evidenced only close to the trailing edge at the mid-span location ($x/c = 0.975$; $z = 0$).

Then, considering the reference gap configuration, it is evident from Figure 9 that no relevant gap effects occur in the mid-span region, whereas along the tip the presence of the gap increases considerably the pressure/velocity correlation and the shape of the velocity signature completely changes with respect to the one occurring in the mid-span region.

5.3 *PIV/pressure conditional statistics*

The joint analysis of PIV measurements (discussed in section 2) and of single point pressure measurements is performed only for the reference gap configuration. On the basis of the HWA/pressure analysis presented above, we may expect the pressure signals recorded by the probe placed at $x/c = 0.75$ to provide the most useful data for the conditional PIV/pressure analyses. Thus, in the present investigation we concentrate primarily on this pressure signal that, once treated with the wavelet method, provides the set of instants from which the corresponding PIV velocity fields are selected.

Contrary to the previous cases, in the present analyses, the pressure signal is processed by using a continuous complex wavelets expansion, so as to achieve a more accurate time frequency resolution. Once the pressure events are extracted at the wall, the conditional analysis has been carried out by averaging together the PIV snapshots corresponding to the selected timing of the wall pressure events. The LIM threshold criterion can be restricted to specific frequency bands in order to select wavelets of a given scale. Examples are shown in the Figure 10 for both low and high frequency containing events. The corresponding flow patterns are identified with the method described above.

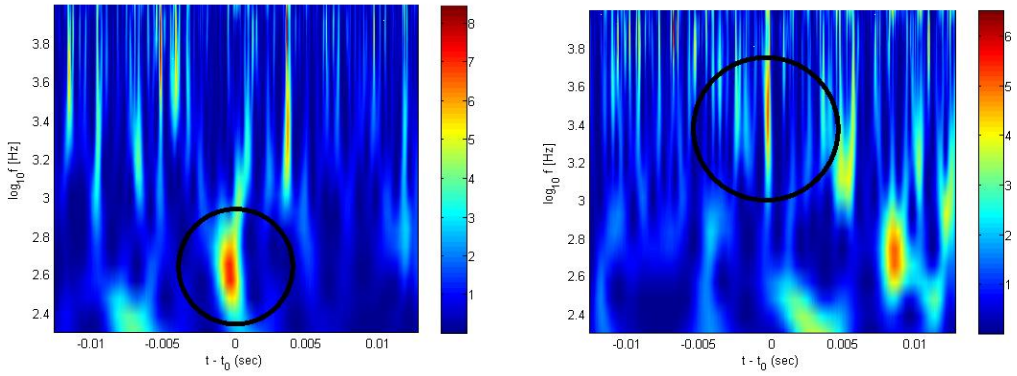

(a) **(b)**

Figure 10. Examples of pressure events (evidenced by the black circle) detected in the wavelet time-frequency domain from the pressure probe located at x/c = 0.75: (a) low-frequency event, (b) high-frequency event.

As stated in section 2, 60 PIV snapshot are available from each 60 sec acquisition series. This represents a basic constraint to take into account, as it is evident that only some of the instantaneous velocity fields captured by these 60 snapshots could be selected. It should be noted that the analyzed pressure segments are centered on the time instants corresponding to the PIV acquisitions timing (see e.g. Figures 12 and 13). Therefore, the selection of a PIV field occurs only

when the LIM peak is located in correspondence of the origin of the time axis which results in a very small number of selected events.
The set of selected velocity fields are eventually averaged together leading to a non-zero averaged tip-flow structure which, should it exist, evidences the most probable fluid dynamic event responsible for the observed large pressure peaks. The selection procedure, applied to all the 10 acquisition series, provided a total of 119 pressure events. Furthermore, as shown on the Figures 10, the LIM peak frequency localization can vary from one case to another. Therefore a distinction has been also considered according to the frequency content of the pressure events (low or high frequencies). Among the 119 events selected, 18 presented a low-frequency behavior, whereas 75 were prevalently associated to high-frequency fluctuations. The remaining 31 fields evidenced events with a broadband frequency content.

The achieved ensemble averaged field corresponding to high frequency events is shown in Figure 11(a). No relevant differences have been evidenced neither when no distinction between high and low frequency events is performed nor when the low-frequency events are considered. In the latter case a lower signal-to-noise ratio is documented due the limited number of samples selected. In any case, in the region upstream of the pressure probe position, thus very close to the region where the source was supposed to act, a non-zero fluid dynamic structure is revealed

The robustness of the results has been verified by the application of the averaging procedure considering the other pressure probe located in the upstream region of the airfoil (see section 2). An example of the achieved averaged field is reported in Figure 11(b) showing that the location of the resulting non-zero structure is consistent with the above presented results.

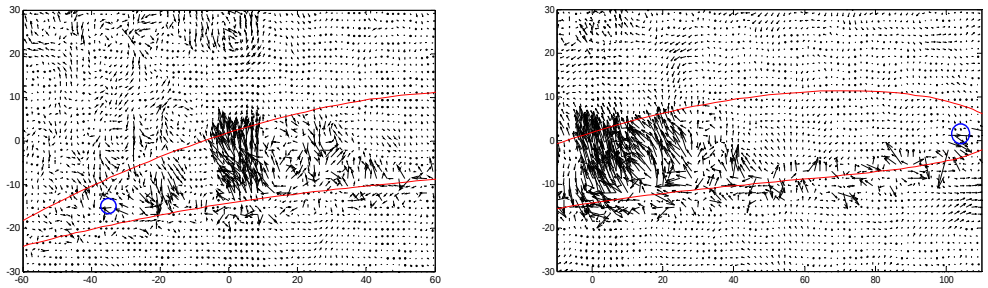

(a) **(b)**

Figure 11. Averaged tip-flow field statistically related to the largest high-frequency pressure fluctuations on the wall. The blue circle denotes the pressure probe utilized in the conditioning procedure. (a) probe located at x/c = 0.75 and (b) probe located at x/c = 0.075.

From the physical viewpoint, this event seems to consist of a motion of the fluid from the pressure side of the airfoil towards the suction side. Actually, since the PIV snapshots are taken in mid-gap plane the figure shows the corresponding 2D cut of the structure. One may assume such structure to be associated to a roll-up phenomenon occurring at the tip edge of the airfoil, but an exact interpretation can not be proposed unless a cross section analysis of the flow is performed.

6 CONCLUSIONS

A detailed analysis of wall pressure and Hot Wire/PIV velocity data measured around an airfoil with and without a tip leakage, have been presented. The post-processing procedure was based on

the application of the wavelet transform to the wall pressure data and the computation of conditional averages of both the pressure and the velocity data. In the self noise configurations, hydrodynamic wall pressure fluctuations have been shown to be mostly related to the boundary layer separation on the suction side near the trailing edge. The presence of a gap leads to quite different behaviors since the most probable fluid dynamic event causing wall pressure peaks is found to be associated to a roll up phenomenon occurring around the tip at 50-60% the chord from the leading edge. The location of the source has been determined from the conditional analysis of the Hot Wire data leading to an averaged structure exhibiting a phase shift with respect to the pressure timing. This result has been definitely confirmed by the conditional analysis of the PIV fields providing a 2D view of the most probable wall pressure source.

7 ACKNOWLEDGMENTS

This work has been funded by the European Community as part of the 6th Framework Project PROBAND n° AST4-CT-2005-012222. R.C. also acknowledge partial support from Italian Ministry of Education, University and Research under a grant PRIN (2005).

References

[1] Mallat, S., "A theory for multiresolution signal decomposition: the wavelet representation", *IEEE Trans.* PAMI 11, 674-693 (1989).

[2] Farge, M., "Wavelet Transforms and their Applications to Turbulence," *Ann. Rev. Fluid Mech.*, **24**, 395-457 (1992).

[3] Camussi, R., Guj, G., "Orthonormal Wavelet Decomposition of Turbulent Flows: Intermittency and Coherent Structures," *Journal Fluid Mech.*, **348**, 177-199 (1997).

[4] Guj, G., Carley, M., Camussi, R., Ragni, A., "Acoustic Identification of Coherent Structures in a Turbulent Jet," *Journal Sound Vibr.*, **259**, 1037-1065 (2003).

[5] Jacob M. C., Grilliat, J., Camussi, R., Caputi-Gennaro, G., "Experimental study of a tip leakage flow – part one: aerodynamic and acoustic measurements", *in Proc. 13th AIAA/CEAS Aeroacoustics Conference*, Rome, Italy, may 21-23 (2007).

[6] Camussi, R., Guj, G., Ragni, A., "Wall Pressure Fluctuations Induced by Turbulent Boundary Layers over Surface Discontinuities," *Journal Sound Vibr.*, **294**, 177-204 (2006).

[7] Camussi, R., Guj, G., Di Marco, A., Ragni, A., "Propagation of Wall Pressure Perturbations in a Large Aspect-Ratio Shallow Cavity," *Exp. Fluids.*, **40**, 612-620 (2006).